Available online at www.sciencedirect.com
SCIENCE DIRECT®
Materials Research Bulletin 39 (2004) 1627–1640
Materials Research Bulletin
www.elsevier.com/locate/matresbu

Synthesis of nanocrystalline zirconia by amorphous citrate route: structural and thermal (HTXRD) studies

Mahesh Bhagwat, Veda Ramaswamy*

National Chemical Laboratory, Catalysis Division, Pune 411004, India

Received 19 November 2003; received in revised form 21 April 2004; accepted 28 May 2004

Abstract

Nanocrystalline zirconia powder with a fairly narrow particle size distribution has been synthesized by the amorphous citrate route. The sample obtained has a high BET surface area of 89 $m^2\,g^{-1}$. Rietveld refinement of the powder X-ray diffraction (XRD) profile of the zirconia sample confirms stabilization of zirconia in the tetragonal phase with around 8% monoclinic impurity. The data show the presence of both anionic as well as cationic vacancies in the lattice. Crystallite size determined from XRD is 8 nm and is in close agreement with the particle size determined by TEM. The in situ high temperature-X-ray diffraction (HTXRD) study revealed high thermal stability of the mixture till around 1023 K after which the transformation of tetragonal phase into the monoclinic phase has been seen as a function of temperature till 1473 K. This transformation is accompanied by an increase in the crystallite size of the sample from 8 to 55 nm. The thermal expansion coefficients are $9.14 \times 10^{-6}\,K^{-1}$ along '*a*'- and $15.8 \times 10^{-6}\,K^{-1}$ along '*c*'-axis. The lattice thermal expansion coefficient in the temperature range 298–1623 K is $34.6 \times 10^{-6}\,K^{-1}$.

Keywords: A. Ceramics; C. X-ray diffraction; D. Crystal structure; D. Thermal expansion

1. Introduction

Use of zirconia as a catalyst and a catalyst support material has increased manifold over the past decade. Where zirconia alone has been exploited as a catalyst in a variety of reactions like alkylation, amination, condensation, isomerisation, cracking, hydration, oxidation, etc. zirconia-mixed oxide systems find even more applications as a catalyst and as a catalyst support [1]. Sulfated zirconia has been explored in catalytic processes owing to its use as a 'super acid' [2]. Researchers have also made attempts to use zirconia as a cathode or a cathode support material for applications

* Corresponding author.
E-mail address: veda@cata.ncl.res.in (V. Ramaswamy).

0025-5408/$ – see front matter © 2004 Elsevier Ltd. All rights reserved.
doi:10.1016/j.materresbull.2004.05.008

in 'solid oxide fuel cells' [3]. Of the three well-defined polymorphs of zirconia, the tetragonal and cubic polymorphs are of more importance for its catalytic applications owing to its properties like high thermal stability, high BET surface area and amphoteric nature. Zirconia exists in monoclinic form at room temperature that gets converted to the tetragonal phase at 1447 K. The tetragonal phase is further converted to the cubic phase at around 2643 K [4–9]. These high temperature tetragonal and cubic phases are, however, unquenchable and obtaining them at lower temperatures has gained importance over the past decade due to their potential applications. Several attempts have been made to obtain the metastable tetragonal and cubic phases by doping zirconia with a variety of metal oxides like CaO, MgO, Y_2O_3, CeO_2, Ce_2O_3, La_2O_3, CuO, MnO_2, NiO, Cr_2O_3, SnO_2, etc. Researchers have explained formation of these metastable phases at low temperature by various theories involving stabilization because of the defects/atomic vacancies in the lattice created by the presence of this lower valent dopent metal ions [10–14]. Synthetic routes like precipitation, sol–gel, ball milling, microwave heating and combustion methods have been tried out successfully to obtain these polymorphs even without adding the dopent metal ions [15–19]. Zirconia obtained by these methods is in the form of nanocrystalline powder, where 'the small crystallite size' plays a key role in stabilizing the zirconia in the tetragonal phase [20].

In our earlier report on the structural characterization of copper-doped zirconia, we observed that both, the concentration of the dopent metal atoms as well as the crystallite size of the powder played significant role in stabilization of zirconia in the tetragonal and the cubic phases [21]. We also studied the effect of temperature on the structural features of the zirconia powders. Our aim has been to study the role of the crystallite size in the stabilization of zirconia into the cubic phase. In the present work, we have prepared 'nanocrystalline' tetragonal zirconia by the amorphous citrate route. This famous Pechini method has been exploited to synthesize a number of single and mixed oxide systems [22] to obtain nanocrystalline powders. It has an advantage over the combustion synthesis because in the combustion synthesis other than the oxide precursors and the fuel, an additional material is required as an oxidant. In the citrate method the citrate complex itself acts as the flux. The product obtained by this route is nanocrystalline with fairly narrow particle size distribution. The amorphous citrate route is a fairly simple technique to produce nanocrystalline powders, less time consuming and cost-effective [23]. The zirconia product obtained by this method has been characterized by powder XRD. Researchers have reported stabilization of zirconia into the tetragonal, cubic and a pseudo-tetragonal or quasi-tetragonal form when nanocrystalline zirconia has been prepared with and without addition of a dopent [24–27]. Further, due to overlapping powder patterns, it becomes difficult to distinguish between the cubic and tetragonal phase when the peak splitting is masked by broad nature of the peak [20]. Hence, Rietveld refinement of the XRD profile was carried out to extract the structural information.

Although zirconia has been studied extensively over a few decades, the research interest on zirconia and related materials is increasing due to the wide range of its growing applications in catalysis and in solid oxide fuel cells where the thermal and structural properties of these materials play an important role. However, very few recent reports about the detailed thermal characterization of these materials could be found. The studies either limit to the use of dilatometric technique to study the bulk thermal expansion or are related to the study of the tetragonal to monoclinic phase transition as a function of temperature, without any quantification or study of the change in lattice parameters or crystallite size as a temperature effect [28–38]. Hence, we have characterized our sample by in situ high temperature XRD (HTXRD) analysis to observe the structural changes as a

function of temperature. The X-ray diffraction (XRD) profiles have been analyzed by the Rietveld refinement technique.

2. Experimental

2.1. Synthesis

Zirconium oxy-nitrate and citric acid (M/S LOBA Chemicals) were taken in a molar ratio of 1:1. Saturated aqueous solutions of both the salts were prepared. The solutions were then mixed and heated on a hot plate at 353 K to obtain a solution of increasing viscosity. Finally, the viscous mass turned into a homogeneous colorless transparent glass. The glass was then heated in a muffle furnace at 673 K for 1 h to obtain an off-white fluffy mass.

2.2. Characterization

Citric acid (used as the precursor), the citrate glass and the zirconia sample obtained by the calcination of the citrate glass were characterized by powder X-ray diffraction technique on a Philips X'Pert Pro 3040/60 diffractometer using Cu Kα radiation ($\lambda = 1.5406$ Å), nickel filter and a proportional counter detector. Silicon was used as the standard to correct the interplanar distance '*d*'. The sample was scanned in the range 20–100°2θ in a step scan mode with a step size of 0.02°. A counting time of 8 s per step was used. The sample was rotated to obtain better counting statistics with the reflection geometry. The powder XRD pattern was refined using the Rietveld refinement technique with the Philips X'Pert Plus software. Crystallite size (L) of the sample was determined using the Scherrer equation, $L = k\lambda/\beta \cos\theta$, where k is the Scherrer constant ($k = 0.9$, assuming that the crystallites are spherical), $\lambda = 1.5406$ Å (Cu Kα radiation), β is the line width and θ is the angle of diffraction. Specific surface area (S) of the samples was calculated from the crystallite size using the formula $S = 6 \times 10^3/L\rho$, where ρ is the density of zirconia. Thermograms and the differential thermograms of the citric acid (used as the precursor) and the amorphous citrate glass were recorded to study their decomposition behaviour. Thermal analysis was carried out on a SETARAM thermal analyzer at a heating rate of 10 K min^{-1} in air atmosphere. The surface area of the sample was measured by the BET method on a NOVA surface area analyzer. The sample was first activated at 573 K to remove moisture and any other volatile matter. Nitrogen gas was used as the adsorbent. TEM micrographs were recorded on a JEOL transmission electron microscope (Model 1200EX) operated at an accelerated voltage of 100 kV.

The zirconia sample was subjected to in situ high temperature powder XRD experiments to observe the structural changes in the sample as a function of temperature. The high temperature powder XRD data were recorded on a Philips X'Pert Pro 3040/60 XRD unit equipped with Anton Paar HTK 1600 attachment. Silicon was used as the standard for calibration. A small amount of sample was mounted on a platinum strip, which serves as the sample stage as well as the heating element. A Pt/Rh–13% thermocouple spot-welded to the bottom of the stage was used for measuring the temperature. The HTXRD patterns were scanned in the 2θ range 20–100° with a step size of 0.02° and a rate of 2° min^{-1}. The patterns were scanned between range 298 K (room temperature) and 1623 K in static air. The powder patterns were recorded at temperature intervals of 150 K from 423 to 1623 K. A heating rate of

10 K min^{-1} and a soak time of 15 min were employed. The XRD profiles were refined by the Rietveld technique to obtain information on the crystallite size, lattice parameters and the phase composition of the mixture.

3. Results and discussion

Nanocrystalline zirconia was obtained by the amorphous citrate route (liquid mix technique). The thermograms and the differential thermograms of the citric acid and the citrate glass are shown in Fig. 1. The thermogram of the citric acid in Fig. 1a shows a major decomposition in the temperature range 318–523 K. A small decomposition in the range 823–923 K could be due to the decomposition of any carbonaceous matter left behind. In Fig. 1b the thermogram of the amorphous citrate glass shows decomposition in three continuous steps. Weight loss in the range 318–416 K could be due to removal of water followed by decomposition of the amorphous citrate glass in two steps between 416 and 579 K and 579 and 752 K. The weight loss in the range 752–869 K could be due to the removal of carbonaceous matter. Difference in the decomposition patterns of the citric acid and the citrate glass clearly indicates formation of a zirconium–citrate complex. During calcination of this citrate glass, a black fluffy mass is obtained which occupies large volumes of the furnace. On increasing the temperature, the black mass turns into loose, off-white powder with removal of carbon. The powder XRD patterns of the citrate glass and the calcination product are given in Fig. 2. Fig. 2a confirms the amorphous nature of the zirconium citrate complex. The powder X-ray diffraction pattern of the calcined sample (Fig. 2b) indicates that it is the mixture of monoclinic and tetragonal polymorphs of zirconia. Broad nature of the peaks indicates nanocrystalline nature of the sample. The powder patterns of the two phases have many overlapping peaks. Hence, Rietveld refinement technique was used to determine the phase composition and analyze the XRD patterns. To verify the presence of cubic phase,

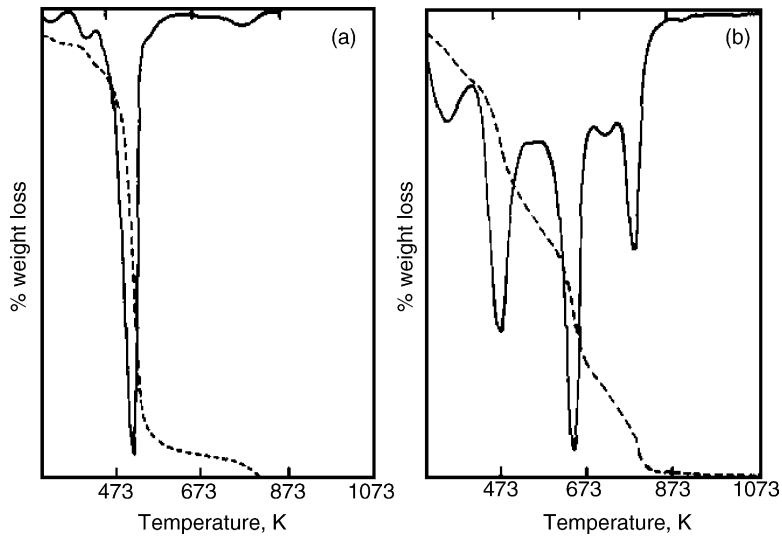

Fig. 1. (a and b) The thermograms and the differential thermograms of the citric acid and the citrate glass.

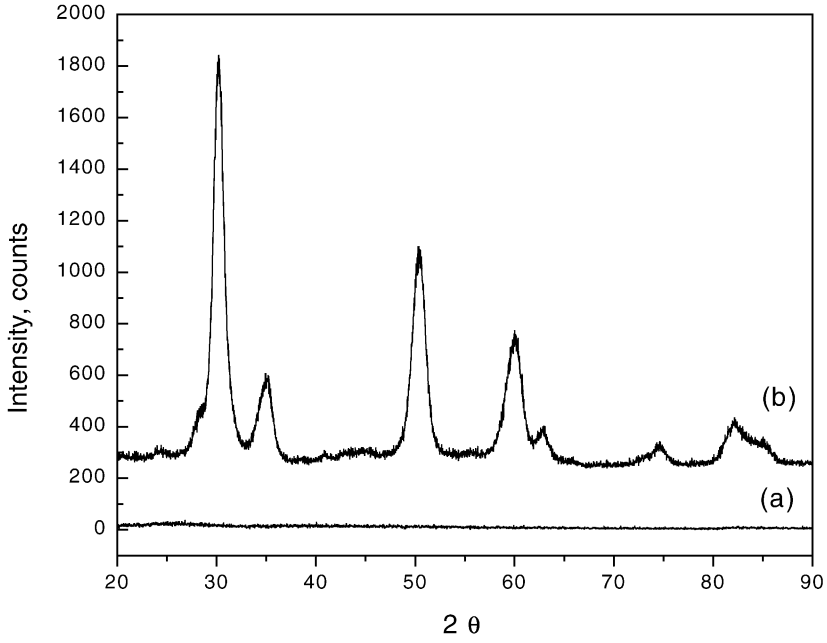

Fig. 2. The powder XRD patterns of citric acid, citrate glass and the calcination product.

the combination of the tetragonal phase with space group $P4_2/nmc$, monoclinic (space group $P2_1/c$) phase and the cubic phase (space group Fm/3m) was used as the starting models for refining. However, it could be observed that the contribution of the cubic phase to the powder pattern was diminishing with the progressive refinement cycles and eventually the results indicated presence of only tetragonal and monoclinic phases in the sample. The refinement was further continued with only the tetragonal and monoclinic phases as the starting models. The background in the pattern was refined using a polynomial with six refinable coefficients. The peak shape was corrected using a Pseudo-Voigt function. The peak width (FWHM) was determined using the equation, $\text{FWHM}=\sqrt{(U + V\tan\theta + W\tan^2\theta)}$ and then the crystallite size was determined using the Scherrer equation. Fig. 3 shows the observed, calculated, and the difference XRD profiles of the sample. The vertical ticks mark the Bragg reflections for both the phases. The refinement revealed tetragonal zirconia as the major phase (92%) with about 8% monoclinic phase. The '*R*' factors obtained from the refinements, the instrumental parameters and the structural information obtained from the refinement of the powder data are listed in Table 1. The sample shows an average crystallite size of about 8 nm (calculated using the Scherrer equation). This small crystallite size could be the important factor in stabilization of zirconia in the tetragonal phase. Refinement of the occupancy factor for zirconium and oxygen atoms showed that the lattice has both cationic as well as anionic vacancies. These lattice defects could also be playing an important role in the stabilization into the tetragonal system along with the small crystallite size Wang et al. [16] has also observed stabilization of zirconia, prepared by two different synthesis routes, into tetragonal phase due to the presence of large scale lattice defects even without addition of any dopents. Model of the crystal structure of tetragonal zirconia simulated using the data obtained from the Rietveld refinement of the XRD pattern is given in Fig. 4. Fig. 5 shows the transmission electron micrographs of

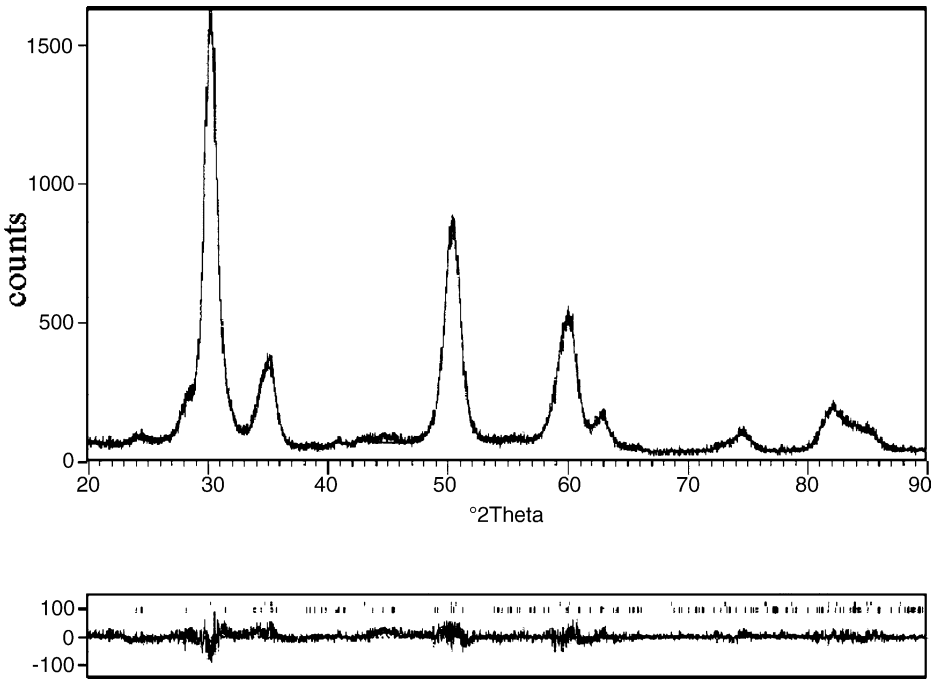

Fig. 3. Rietveld refinement profiles of zirconia scanned at room temperature. The observed (-), calculated (. . .) and the difference (+++) XRD profiles of the sample. The vertical ticks indicate Bragg reflections for the monoclinic and the tetragonal phases.

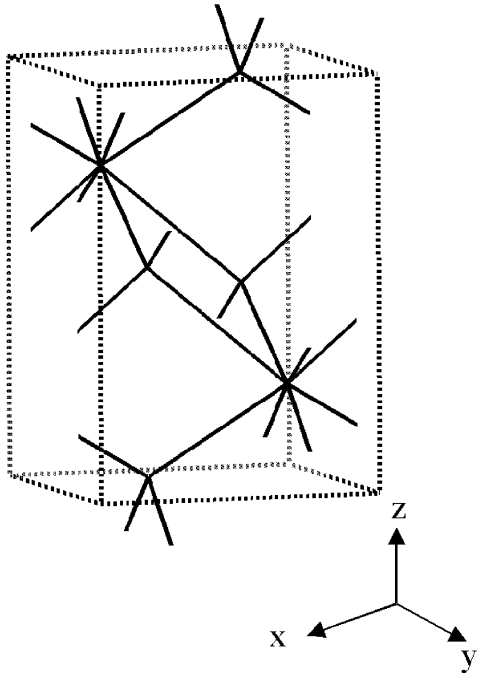

Fig. 4. Structural model of tetragonal zirconia.

Table 1
Structural data of zirconia obtained from Rietveld refinement

Crystal system	Tetragonal			
Space group	$P4_2/nmc$			
Formula	$ZrO_{2-\delta}$			
Weight fraction	92%			
Temperature	298 K			
Unit cell dimensions	a (nm)	0.359 (6)		
	c (nm)	0.516 (7)		
	V (nm)^3	6.815 (2)		
	$\alpha = \beta = \gamma$	90°		
Atom	Occupancy	x	Y	Z
Zr	0.88 (5)	0.75	0.25	0.75
O	0.89 (2)	0.25	0.25	0.4462(5)
Distances and angles	Zr–O (nm)	0.206 (9)		
	Zr–O (nm)	0.238 (4)		
	O–Zr–O	132.0 (6)°		
R-factors	R_{EXP} (%)	8.392		
	R_P (%)	7.28		
	R_{WP} (%)	10.466		
	R_B (%)	1.196		
	GOF (χ^2)	1.247		

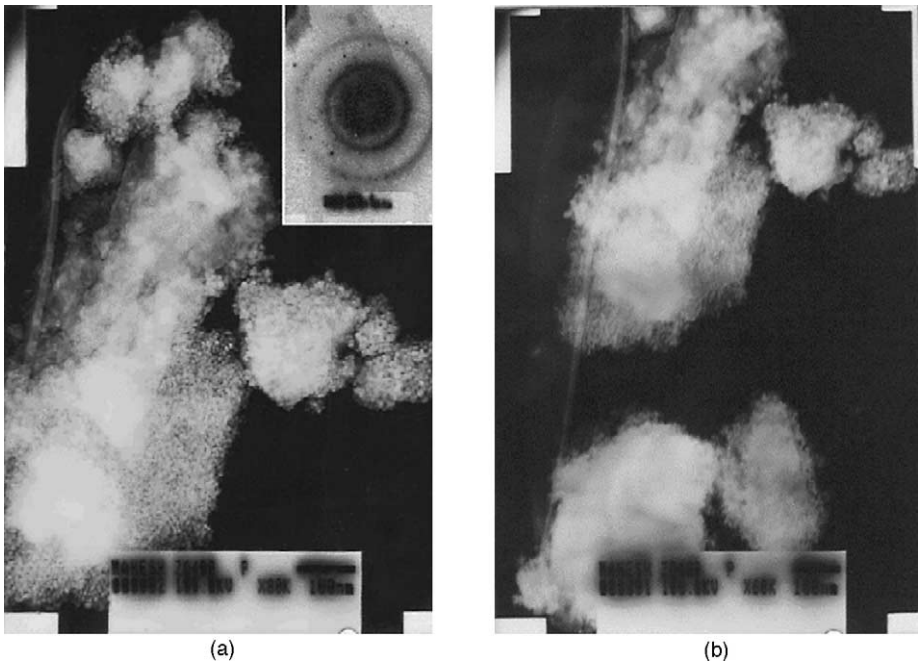

Fig. 5. (a and b) Transmission electron micrographs of the sample. Electron diffraction pattern is given in the inset.

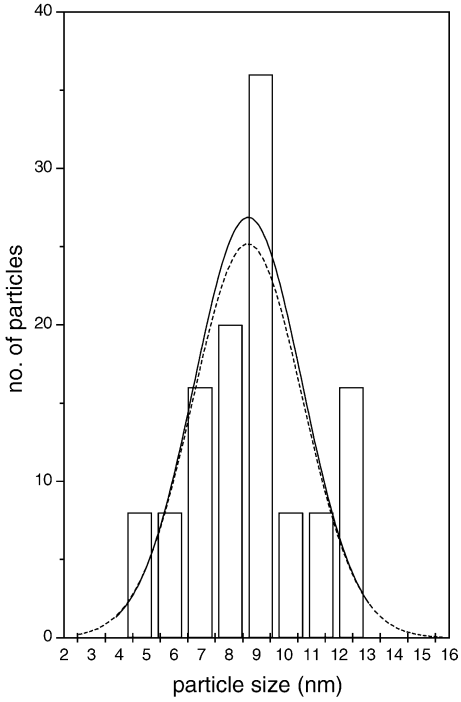

Fig. 6. Histogram of the particle size distribution as obtained from the TEM.

the sample. The micrographs show large aggregates of zirconia particles varying from 50 to 100 nm. Each aggregate contains homogeneous distribution nanocrystalline zirconia particles. The electron diffraction pattern is given in the inset. The diffused pattern indicates a short-range order in the sample. The particle size distribution is represented in the histogram given in Fig. 6. The distribution seems to be fairly narrow between 4 and 10 nm, with the maximum particles at about 9 nm (±2 nm). The results are comparable to the crystallite size obtained from the powder XRD data (8 nm). This suggests that each particle is as good as a single crystal with an order of about 8–18 unit cells along each of the three crystallographic axes. The sample has a BET surface area of the sample (89 $m^2\ g^{-1}$) obtained by the nitrogen adsorption experiment. The BET surface area is comparable to the specific surface area (97 $m^2\ g^{-1}$) calculated from the crystallite size. It has been reported that the stabilization of zirconia into the cubic phase and the tetragonal phase is favored by higher concentration of dopent metal and smaller crystallite size [21]. In the present study we have seen that the smaller crystallite size, along with the presence of lattice defects seems to be responsible for stabilization of zirconia into the tetragonal phase without any metal doping.

3.1. HTXRD data

Fig. 7 gives the multiple plot of the high temperature powder XRD profiles of the sample scanned between room temperature (298 K) and 1623 K. The HTXRD profiles were subjected to Rietveld refinement technique to obtain information about the change in the phase composition, crystallite size

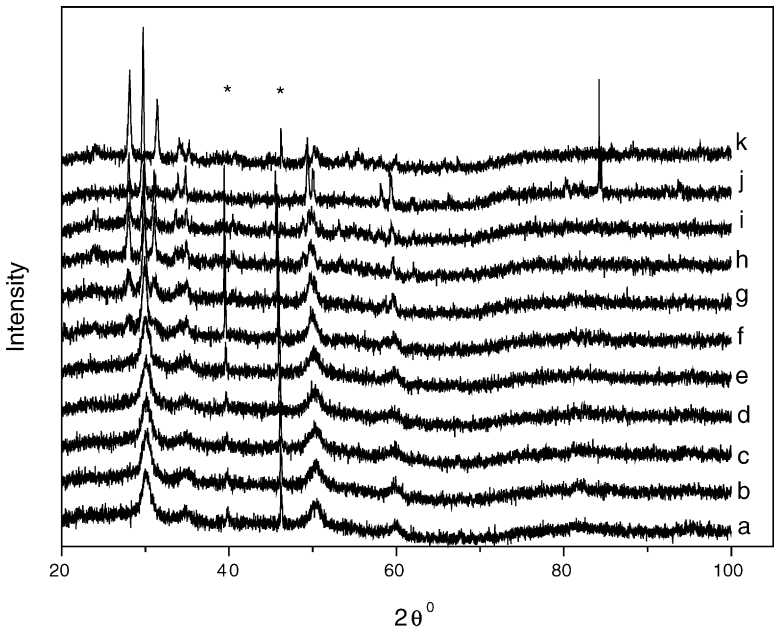

Fig. 7. Multiple plot of the HTXRD profiles of the sample scanned from 298 to 1623 K. (a) 298 K, (b) 423 K, (c) 573 K, (d) 723 K, (e) 873 K, (f) 1023 K, (g) 1173 K, (h) 1323 K, (i) 1473 K, (j) 1623 K, (k) room temperature scan on cooling back. (*) indicate peaks due to platinum.

and lattice parameters of the sample as a function of temperature. However, because of the poor counting statistics of the HTXRD fast scan, the data could not be exploited for determining the structural parameters of the phases and the cationic and anionic vacancies in the sample. Fig. 8 shows variation of the relative phase composition of the polymorph mixture as a function of temperature. The data indicate that the composition (92% tetragonal and 8% monoclinic) is stable up to 873 K (Fig. 7e). Above 873 K, the tetragonal phase gets transformed into the monoclinic phase. From 1023 to 1473 K there is a decrease in the relative percentage of the tetragonal phase from 90 to 30%. The data suggest high thermal stability of the tetragonal phase. Complete transformation of the tetragonal phase into the monoclinic phase was not seen. At 1623 K, the expected martensitic transformation of the monoclinic phase into the tetragonal phase can be observed. At 1623 K, only the highly crystalline tetragonal phase exists. Fig. 7k shows the powder pattern scanned at room temperature after the HTXRD scan. The pattern shows presence of only the monoclinic phase indicating complete transformation of the tetragonal to monoclinic phase on cooling the sample to room temperature. Fig. 9 shows the change in crystallite size and the relative percentage of the tetragonal phase with temperature. It can be observed that the crystallite size remains constant (8 nm) till 873 K and so does the relative percentage of the tetragonal phase (90%). From 1023 to 1473 K, the crystallite size increases from 25 to 55 nm with a decrease in the relative percentage of the tetragonal phase from 85 to 25%. Decrease in relative concentration of the tetragonal phase with sintering of the zirconia crystallites clearly indicates that stabilization of zirconia in the tetragonal phase is a function of the crystallite size. We had observed similar results in our earlier study on stabilization of zirconia by copper doping [21]. A simultaneous increase in the crystallite size of the monoclinic phase was observed in the temperature range 1023–1473 K.

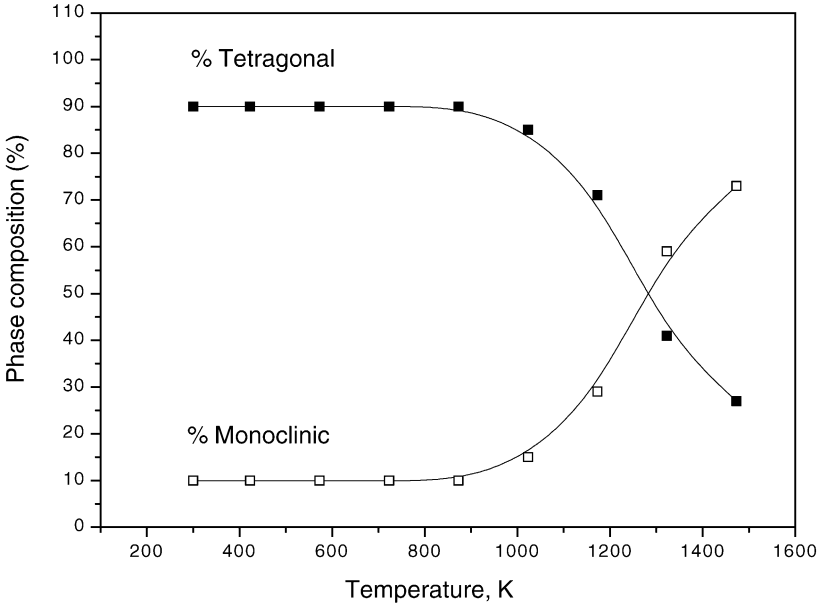

Fig. 8. Variation of the relative phase composition of the polymorph mixture as a function of temperature.

The change in lattice parameters '*a*' and '*c*' and change in the unit cell volume '*V*' of the tetragonal phase as a function of temperature are plotted in Fig. 10a and b, respectively. The plot shows a linear increase in the values of the lattice parameters '*a*' and '*c*' and hence an increase in the unit cell volume as a function of temperature can be observed. The percent thermal expansion along the '*a*'-axis ($100 \times \Delta a/a$) and '*c*'-axis ($100 \times \Delta c/c$) and the percent lattice thermal expansion ($100 \times \Delta V/V$) at each

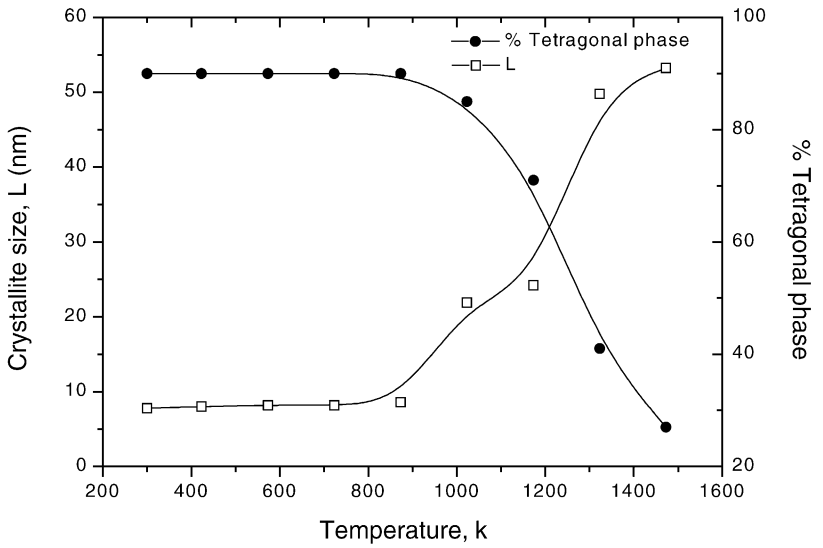

Fig. 9. Change in the crystallite size and the relative percentage of the tetragonal phase with temperature.

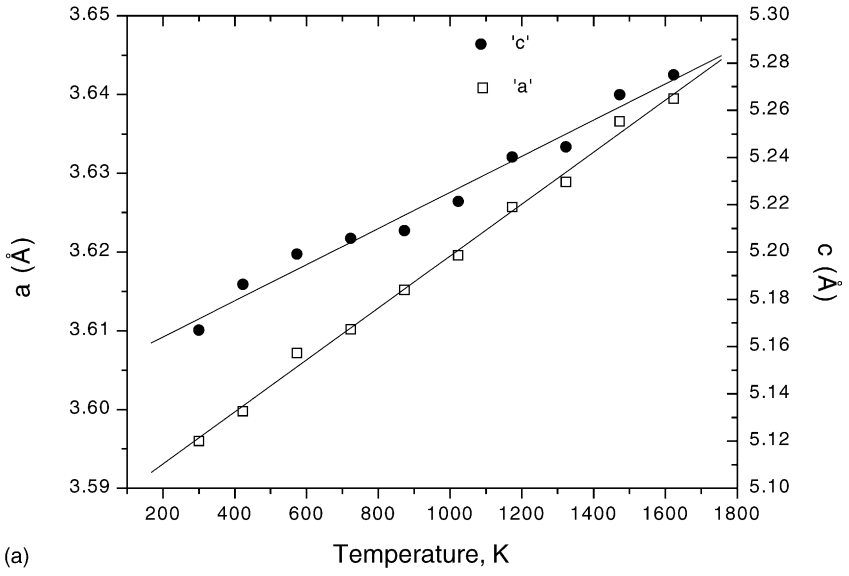

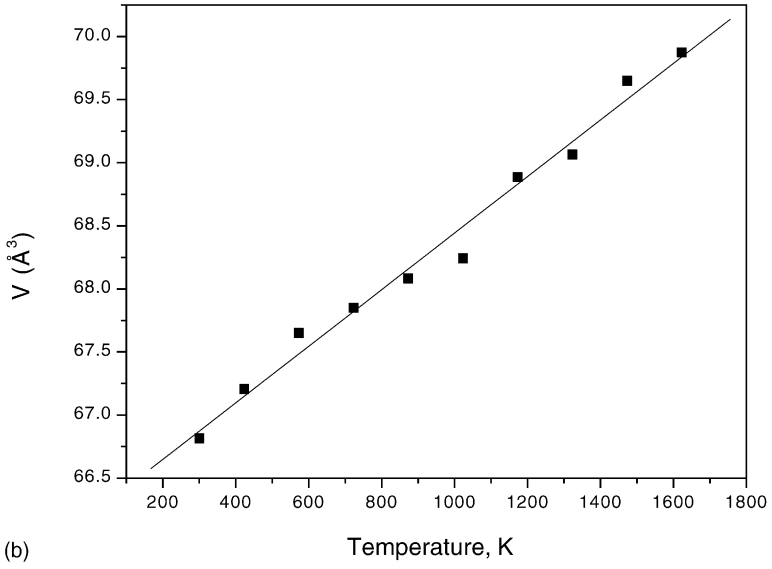

Fig. 10. (a and b) The change in lattice parameters '*a*' and '*c*' and the unit cell volume '*V*' of the tetragonal phase as a function of temperature.

temperature were calculated. The change in the percent thermal expansion along '*a*' and '*c*', and the percent lattice thermal expansion as a function of temperature are given in Fig. 11a and b, respectively. There is a linear increase in the percent thermal expansion along '*a*' and '*c*' as well as the percent lattice thermal expansion. The data indicate a maximum of 1.2% expansion along '*a*' and 2.1% along '*c*' at temperature 1623 K. The maximum percent lattice thermal expansion (in terms of expansion of

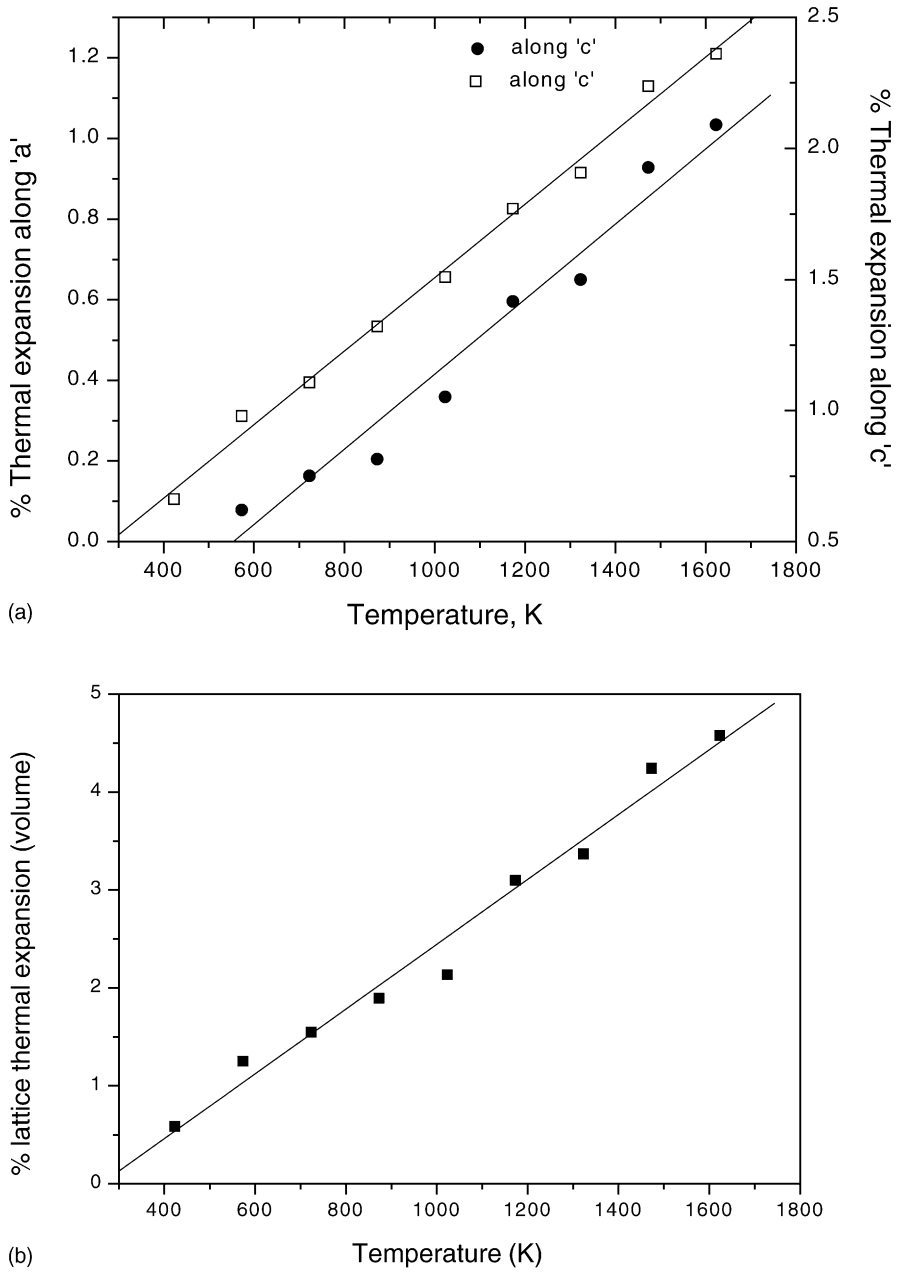

Fig. 11. (a and b) The change in the percent thermal expansion along '*a*' and '*c*', and the percent lattice thermal expansion a function of temperature.

the unit cell volume) is about 4.6% at 1623 K. Table 2 gives the thermal expansion coefficient along '*a*' (α_a) and '*c*' (α_c) and lattice thermal expansion coefficient (α_V) calculated using the following equations.

$$\alpha_a = \frac{\Delta a}{(T - \mathrm{RT})a_{\mathrm{RT}}}$$

Table 2
Unit cell volume and coefficient of lattice thermal expansion in the temperature range of 298–1623 K

Temperature (K)	Unit cell volume V (Å^3)	$\alpha_V = \Delta V/(T - \mathrm{RT})V_{\mathrm{RT}} \times 10^{-6}\,\mathrm{K}^{-1}$
298	66.815(2)	–
423	67.206(7)	47.66
573	67.650(1)	45.78
723	67.849(9)	36.62
873	68.081(5)	33.08
1023	68.240(9)	29.52
1173	68.885(4)	35.5
1323	69.064(7)	32.91
1473	69.649(1)	36.16
1623	69.876(5)	34.6

Values given in the parentheses refer to the E.S.D.

$$\alpha_a = \frac{\Delta c}{(T - \mathrm{RT})c_{\mathrm{RT}}}$$

$$\alpha_a = \frac{\Delta V}{(T - \mathrm{RT})V_{\mathrm{RT}}}$$

where RT is the room temperature (298 K) and T is the temperature at which the measurements were done. The average thermal expansion coefficient between the range 298–1623 K is $9.14 \times 10^{-6}\,\mathrm{K}^{-1}$ along 'a' and $11.58 \times 10^{-6}\,\mathrm{K}^{-1}$ along 'c'. The average lattice thermal expansion coefficient in the temperature range 298–1623 K is $34.62 \times 10^{-6}\,\mathrm{K}^{-1}$.

4. Conclusions

Nanocrystalline zirconia powder with a fairly narrow particle size distribution can be obtained by the amorphous citrate route. The powder obtained has a high surface area of $89\,\mathrm{m}^2\,\mathrm{g}^{-1}$. Rietveld refinement of the powder XRD profile of the zirconia sample suggests stabilization of zirconia in the tetragonal phase with around 8% monoclinic impurity. Smaller crystallite size plays a role in the stabilization of zirconia into the tetragonal phase. Presence of both anionic as well as cationic vacancies are observed. The in situ HTXRD study reveals high thermal stability of the mixture till around 1023 K after which the transformation of tetragonal phase into the monoclinic phase can be seen as a function of temperature till 1473 K. This transformation is accompanied by an increase in the crystallite size of the sample. A linear increase in the lattice parameters and percent thermal expansion as a function of temperature indicates a linear lattice thermal expansion.

Acknowledgements

V.R. is thankful to Department of Science and Technology, New Delhi for the financial support. M.B. is grateful to CSIR, New Delhi for the Senior Research Fellowship.

References

[1] T. Yamguchi, Catal. Today 20 (1994) 199–218.
[2] K. Arata, Adv. Catal. 37 (1990) 165.
[3] E.C. Subbarao (Ed.), Solid Electrolytes and Their Applications, Plenum Press, New York, 1980.
[4] R. Stevens, Zirconia, second ed., Magnesium Electrons Ltd., 1986.
[5] S.K. Saha, P. Pramanik, Br. Ceram. Trans. 94 (1995) 123.
[6] C.F. Grain, J. Am. Ceram. Soc. 56 (4) (1967) 288.
[7] R.P. Ingel, D. Lewis III, J. Am. Ceram. Soc. 69 (4) (1986) 325.
[8] H. Ishizawa, O. Sakurai, N. Mizutani, M. Kato, Am. Ceram. Soc. Bull. 65 (1986) 1399.
[9] A.M. George, N.C. Mishra, N.C. Jayadevan, J. Mater. Sci. Lett. 11 (1992) 404.
[10] R.C. Garvie, J. Phys. Chem. 69 (4) (1965) 1238.
[11] R.C. Garvie, J. Phys. Chem. 82 (4) (1978) 218.
[12] V.S. Stubican, J.R. Hellman, in: Adv. Ceramics, III, Science and Technology of Zirconia, 1981, p. 25.
[13] M. Yashima et al., Acta Cryst. BSD 663.
[14] A. Clearfield, J. Mater. Res. 5 (1) (1990) 161.
[15] S. Roy, J. Ghose, Mater. Res. Bull. 35 (2000) 1195.
[16] J.A. Wang, M.A. Valenzuela, J. Salmones, A. Vazquez, A.- Ruiz, X. Bokhimi, Catal. Today 68 (2001) 21.
[17] J. Liang, X. Jiang, Z. Deng, J. Zhuang, F. Li, Y. Li, Mater. Res. Bull. 38 (2003) 161–168.
[18] R.E. Juarez, D.G. Lamas, G.E. Lascalea, N.E. Walsoe de Reca, J. Eur. Ceram. Soc. 20 (2000) 133.
[19] E. Djurado, E. Meunier, J. Solid State Chem. 141 (1998) 191.
[20] R. Gravie, J. Phys. Chem. 69 (4) (1965) 1238.
[21] M. Bhagwat, A.V. Ramaswamy, A.K. Tyagi, V. Ramaswamy, Mat. Res. Bull. 38 (2003) 1713–1724.
[22] M.P. Pechini, US Patent, 3 330 (1967) 697.
[23] M. Bhagwat, P. Shah, V. Ramaswamy, Mater. Lett. 57 (2003) 1604.
[24] M.K. Dongare, V. Ramaswamy, C.S. Gopinath, A.V. Ramaswamy, S. Scheurell, M. Brueckner, E. Kemnitz, J. Catal. 199 (2001) 209.
[25] D.G. Lamas, N.E. Walsue De Reca, in: Proceedings of the 22nd International Symposium on Materials Science, Denmark, 2001, p. 313.
[26] J.A. Wang, M.A. Valenzuela, J. Salmones, A. Vazguez, A. Garcia Ruiz, X. Bokhimi, Catal. Today 68 (2001) 21.
[27] D.G. Lamas, N.E. Walsue De Reca, Mater. Lett. 41 (1999) 204.
[28] A.A.M. Ali, M.I. Zaki, Thermochim. Acta 336 (1999) 17.
[29] Y. Shiratori, F. Tietz, H.P. Buchkremer, D. Stover, Solid State Ionics 164 (1–2) (2003) 27.
[30] H. Tsubakino, N. Matsuura, J. Am. Ceram. Soc. 85 (8) (2002) 2102.
[31] M.K. Naskar, M. Chatterjee, D. Ganguli, Bull. Mater. Sci. 25 (5) (2002) 413.
[32] S. Yoneda, Y. Ohno, Adv. Sci. Technol. 33 (2003) 77.
[33] C. Wan, Y. Motohashi, S. Harjo, Mater. Trans. 44 (5) (2003) 1053.
[34] J.-L. Bechade, R. Brenner, P. Goudeau, M. Gailhanou, Mater. Sci. Forum 404 (2002) 803.
[35] M.J. Bannister, S. Rajendran, Mater. Sci. Forum 34 (1988) 207.
[36] T.S. Sheu, J. Am. Ceram. Soc. 76 (7) (1993) 1772.
[37] B. Basu, L. Donzel, J. Van Humbeeck, J. Vleugels, R. Schaller, B.O. Van Der, Scripta. Mater. 40 (7) (1999) 759.
[38] O. Liu, S. An, W. Qiu, Solid State Ionics 1211 (4) (1999) 61.